The American Journal of Pathology, Vol. 184, No. 1, January 2014

ELSEVIER

The American Journal of
PATHOLOGY
ajp.amjpathol.org

MOLECULAR PATHOGENESIS OF GENETIC AND INHERITED DISEASES

Dysferlin and Myoferlin Regulate Transverse Tubule Formation and Glycerol Sensitivity

Alexis R. Demonbreun,* Ann E. Rossi,* Manuel G. Alvarez,† Kaitlin E. Swanson,† H. Kieran Deveaux,* Judy U. Earley,* Michele Hadhazy,* Ravneet Vohra,‡ Glenn A. Walter,‡ Peter Pytel,† and Elizabeth M. McNally*§

From the Departments of Medicine, Pathology,† and Human Genetics,§ The University of Chicago, Chicago, Illinois; and the Department of Physiology and Functional Genomics,‡ University of Florida, Gainesville, Florida*

Accepted for publication September 16, 2013.

Address correspondence to Elizabeth M. McNally, M.D., Ph.D., The University of Chicago, 5841 S Maryland, MC6088, Chicago, IL 60637. E-mail: emcnally@uchicago.edu.

Dysferlin is a membrane-associated protein implicated in muscular dystrophy and vesicle movement and function in muscles. The precise role of dysferlin has been debated, partly because of the mild phenotype in dysferlin-null mice (*Dysf*). We bred *Dysf* mice to mice lacking myoferlin (*MKO*) to generate mice lacking both myoferlin and dysferlin (FER). FER animals displayed progressive muscle damage with myofiber necrosis, internalized nuclei, and, at older ages, chronic remodeling and increasing creatine kinase levels. These changes were most prominent in proximal limb and trunk muscles and were more severe than in *Dysf* mice. Consistently, FER animals had reduced ad libitum activity. Ultrastructural studies uncovered progressive dilation of the sarcoplasmic reticulum and ectopic and misaligned transverse tubules in FER skeletal muscle. FER muscle, and *Dysf*- and *MKO*-null muscle, exuded lipid, and serum glycerol levels were elevated in FER and *Dysf* mice. Glycerol injection into muscle is known to induce myopathy, and glycerol exposure promotes detachment of transverse tubules from the sarcoplasmic reticulum. Dysf, *MKO*, and FER muscles were highly susceptible to glycerol exposure *in vitro*, demonstrating a dysfunctional sarcotubule system, and *in vivo* glycerol exposure induced severe muscular dystrophy, especially in FER muscle. Together, these findings demonstrate the importance of dysferlin and myoferlin for transverse tubule function and in the genesis of muscular dystrophy. *(Am J Pathol 2014, 184: 248–259; http://dx.doi.org/10.1016/j.ajpath.2013.09.009)*

The muscular dystrophies are a heterogeneous group of genetic disorders characterized by progressive muscle loss and weakness. The mechanisms that underlie muscular dystrophy are diverse, including defective regeneration, plasma membrane instability, and defective membrane repair. Dysferlin (DYSF) has been implicated in all of these processes.[1,2] Autosomal recessive loss-of-function mutations in dysferlin cause three different forms of muscular dystrophy: limb-girdle muscular dystrophy type 2B, Miyoshi myopathy, and distal anterior compartment myopathy.[3–5] Mutations in dysferlin become clinically evident in the second to third decade or later, with muscle weakness. An early characteristic feature of dysferlin mutations is massively elevated serum creatine kinase levels. A spectrum of myopathic changes can be seen in muscle biopsy specimens from humans with dysferlin mutations, including dystrophic features, such as fibrofatty replacement and inflammatory infiltrates.

Dysferlin is a 230-kDa membrane-inserted protein that contains at least six cytoplasmic C2 domains. C2 domains mediate protein-protein interactions and, in some cases, directly bind phospholipids and calcium. The C2 domains of dysferlin are highly related to those found in the membrane trafficking and fusion protein synaptotagmins.[6] Dysferlin is highly expressed in adult skeletal muscle, whereas it is expressed at lower levels in muscle precursor cells, myoblasts.[1,7,8] On sarcolemma damage, dysferlin is found at the sites of membrane disruption and has been specifically implicated in resealing the sarcolemma.[2] Electron microscopy of skeletal muscle biopsy specimens from human dysferlin-mutant patients confirms discontinuity of the

Supported by the NIH through the National Institute of Neurological Diseases and Stroke grant R01 NS047726, the National Institute for Arthritis and Musculoskeletal and Skin Diseases grant U54 AR052646, and the Muscular Dystrophy Association (E.M.M.).

http://dx.doi.org/10.1016/j.ajpath.2013.09.009

sarcolemma and reveals vesicles underneath the basal lamina, suggesting dysferlin plays an active role in vesicle fusion at the membrane lesion.[9] Dysferlin also has been shown to interact with a variety of cytosolic and membrane-associated binding partners, including MG53, caveolin-3, AHNAK, and annexins A1 and A2.[10–13] Similar to dysferlin, MG53, caveolin-3, and the annexins have been implicated in membrane resealing, suggesting a large complex may act coordinately to seal the disrupted plasma membrane in a calcium-dependent manner.[13,14]

An increasing body of evidence suggests that dysferlin's membrane-associated roles are not restricted to the sarcolemma. Dysferlin has been implicated in the development and maintenance of the transverse (T-) tubule, a muscle-specific membrane system essential for electromechanical coupling. The T-tubule is a membrane inversion of the sarcolemma that flanks the Z band of muscle, the anchor for sarcomeric proteins. Dysferlin associates with the T-tubule–like system in differentiated C2C12 myotubes,[15] and dysferlin-null mouse muscle contains malformed T-tubules consistent with a role for dysferlin in the biogenesis and maintenance of the T-tubule system.[16] In mature muscle damaged by stretch, dysferlin localizes to T-tubules, suggesting a reparative function for dysferlin at the T-tubule.[17]

Dysferlin belongs to a family of proteins, the ferlins, that contains six family members. Myoferlin is a dysferlin homologue, which is 76% identical at the amino acid level.[18] Such as dysferlin, myoferlin also contains at least six calcium-sensitive C2 domains, a carboxy-terminal transmembrane domain, an Fer domain, and a DysF domain.[17,19] Myoferlin is highly expressed in myoblasts and is markedly up-regulated in adult skeletal muscle on muscle damage.[20] Myoferlin, such as dysferlin, is required for normal myoblast fusion and muscle growth through regulating steps of vesicle trafficking and endocytic recycling.[1,20,21] Myoferlin, such as dysferlin, is required for the proper trafficking of and response to the insulin-like growth factor-1 receptor in muscle.[22] Myoferlin interacts with endocytic recycling proteins EHD1 and EHD2, as well as AHNAK.[21,23,24] To date, no human forms of muscular dystrophy resulting from myoferlin mutations have been reported. However, mice lacking myoferlin show defects in muscle regeneration, establishing a role for myoferlin in muscle repair.[20]

We generated ferlin (FER) mice that carry both the dysferlin- and myoferlin-null loss of function mutations. We determined that FER mice have a more severe muscular dystrophy than dysferlin-null mice. In addition, FER muscle displays disorganization of the T-tubule system, dilated sarcoplasmic reticulum, and increased levels of serum glycerol. We revealed an enhanced sensitivity of *Dysf*, *MKO*, and especially FER myofibers to glycerol exposure, resulting in T-tubule vacuolation and disrupted membrane potential. Intramuscular glycerol injections into young FER muscle recapitulated the dystrophic phenotype characteristic of old FER muscle. Our data establish a role for both myoferlin and dysferlin in the biogenesis and remodeling of the sarcotubule system and suggest glycerol as a mediator of muscular dystrophy in dysferlin mutations.

Materials and Methods

Generation of FER Mice

The naturally occurring dysferlin-null mice from the A/J strain were backcrossed for six generations to the 129/SV emst/J myoferlin mouse line, to generate FER mice with both the *Dysf* and *MKO* alleles.[20,25] Mice were housed in a specific pathogen-free facility in accordance with the University of Chicago (Chicago, IL) Institutional Animal Care and Use Committee regulations.

Muscle Fiber Analysis

Muscles from 24-week-old mice were dissected and frozen in liquid nitrogen–cooled isopentane. Muscle sections were stained with H&E or anti-dystrophin (Ab15277; Abcam, Cambridge, MA), diluted 1:200. By using ImageJ (NIH, Bethesda, MD) particle analysis, the mean area was determined from >275 fibers from at least five fields from three different animals per genotype. The percentage of fibers with central nuclei was calculated from the number of fibers containing internalized nuclei in each image/the total number of fibers counted per image, standardized as a percentage. At least 2000 fibers per genotype were analyzed ($n = 3$ from each genotype). Statistical analysis was performed using Prism version 4 (Graphpad, La Jolla, CA). Images were captured using a Zeiss Axiophot microscope.

Muscle Analysis

Quadricep, tricep, abdominal, paraspinal, gluteus/hamstring, and gastrocnemius/soleus muscles from age-matched, wild-type (WT), *Dysf*, mice lacking myoferlin (*MKO*), and FER animals were dissected and frozen in liquid nitrogen–cooled isopentane ($n \geq 3$ animals per genotype per age). Muscle sections were stained with H&E. Images were captured using a Zeiss Axiophot microscope.

Creatine Kinase and Metabolite Assays

Serum was collected from age-matched, WT, *Dysf,* MKO, and FER animals from eye bleeds using heparinized capillary tubes (Fisher, Pittsburgh, PA) into serum separator tubes (Becton Dickinson, Franklin Lakes, NJ) and centrifuged for 10 minutes at 8000 × *g*. The plasma fractions were frozen and stored at −80°C and then assayed later using the EnzyChrom CK Assay kit (ECPK-100; BioAssay Systems, Hayward, CA). Serum glycerol was determined with the Cayman Chemical Assay kits (number 10010755; Cayman Chemical, Ann Arbor, MI). Activity was measured in the FluoStar Optima plate reader (BMG Labtech, Cary, NC).

Free-Running Wheel Analysis

Sixteen-month-old WT, *Dysf,* MKO, and FER mice were housed individually and were allowed to run on a free-running wheel over a period of 48 hours (ENV-004; Med Associates, St. Albans, VT). Wheel-running activity was continuously monitored through wireless transmitters and recorded using the Wireless Running Wheel Manager Data Acquisition Software version 1.5 (SOF-860; Med Associates). Wheel activity was analyzed from 5 PM to 5 AM in 1-minute bins. Mean wheel rotations were calculated from at least two nights. Kilometers per minute was calculated from the average kilometers per minute during activity.

Immunofluorescence Microscopy

Quadricep muscles from 6-month-old, WT, *Dysf*, MKO, and FER mice were divided into sections and fixed with 4% paraformaldehyde blocked in 1× PBS containing 10% fetal bovine serum, and then immunostained. Anti-sarcoplasmic endoplasmic reticulum calcium ATPase (SERCA) 1 (clone CaF2-5D2; Developmental Studies Hybridoma Bank, Iowa City, IA) was used at a dilution of 1:100, and anti-dystrophin was used at a dilution of 1:200 (Ab15277; Abcam). Goat anti-mouse Alexa 594 (number A11005; Invitrogen, Grand Island, NY) was used at a dilution of 1:5000, and goat anti-rabbit Alexa 488 antibody (number A11008; Invitrogen) was used at a dilution of 1:5000. Slides were mounted with Vectashield (Burlingame, CA) with DAPI. Images were captured using a Zeiss Axiophot microscope.

Immunoblotting

Proteins transferred to membranes were immunoblotted with anti-annexin A2 used at a dilution of 1:3000 (number 610068; BD Transduction, Franklin Lakes, NJ), rabbit polyclonal anti-Fer1L5 antibody[23] was used at a dilution of 1:3000, anti-dihydropuridine receptor (DHPR) (MA3-920; Pierce, Rockford, IL) was used at a dilution of 1:3000, and anti−caveolin-3 (number 610420; BD Transduction) was used at a dilution of 1:1000. Secondary antibodies, goat anti-rabbit and goat anti-mouse conjugated to horseradish peroxidase (Jackson ImmunoResearch, West Grove, PA), were used at a dilution of 1:5000. Blocking and antibody incubations were performed in StartingBlock T20 (Tris-buffered saline) Blocking Buffer (Pierce). ECL-Plus chemiluminescence (GE Healthcare, Piscataway, NJ) and Kodak Biomax MS film were used for detection.

FDB Preparation and Immunofluorescence Microscopy

WT and FER flexor digitorum brevis (FDB) muscle was removed and incubated in collagenase II (number 17101-015; Invitrogen). After 2 to 3 hours, FDB bundles were moved to media containing 3% bovine serum albumin and 0.1% gentamicin for trituration. Free fibers were incubated at 37°C overnight and plated on Matrigel (number 356234; BD Bioscience) coated coverslips. Fibers were fixed in 4% paraformaldehyde, rinsed, and blocked in Super Block (number 37515; Pierce) with 0.1% Triton X-100 (Sigma, St. Louis). Anti-DHPR (number MA3-920; Pierce) was used at a dilution of 1:100. Goat anti-mouse Alexa 488 (number A11001; Invitrogen) was used at a dilution of 1:2000. Slides were mounted in Vectashield with DAPI. Images were acquired on the Marianas Yokogawa spinning disk confocal using a 100× oil objective.

Glycerol Injections

By using a standard aseptic surgery procedure, the tibialis anterior (TA) muscles from 8-week-old mice were injected with 50% or 1% glycerol mixed with HBSS (number 14025-092; Gibco, Grand Island, NY) with a sterile insulin syringe, as previously described.[26] Mice were sacrificed at 5 or 28 days after injection. Muscles were dissected and frozen in liquid nitrogen−cooled isopentane.

Glycerol Fiber Assay and T-Tubule Analysis

FDB fibers were isolated from 8-week-old, WT, *Dysf*, MKO, and FER mice and plated on corning plates in Ringer's solution in 2 mmol/L calcium. Fibers were stained with 10 μmol/L RH414 for 15 minutes before imaging at room temperature. Ringer's solution with 100 mmol/L glycerol and 10 μmol/L RH414 (catolog no. T-1111; Molecular Probes, Grand Island, NY) was placed on the preloaded fibers for 30 minutes, whereas healthy fibers were located on the Marianas Yokogawa spinning disk confocal using a 100× oil objective (561 nm, 100 milliseconds, neutral density 20) and bright field (100 milliseconds, neutral density 20).[27] After 30 minutes, the Ringer's glycerol mixture was washed out using a gravity perfusion system and the solution was replaced with normal Ringer's solution. Images were acquired immediately after washout. Images were taken every 1 minute for 15 minutes, 7 μm from the cell surface. Confocal images of WT, MKO, DYSF, and FER fibers, loaded with RH414 at time 0 and 15 minutes after glycerol withdrawal, were used to generate plot profiles, which were analyzed in Sigview (SignalLab) to calculate the fast Fourier transformation of the RH414 signal. The amplitude of the peak in the power spectrum correlates with the amount of regular T-tubule RH414 signal at the z-lines. The signal between peaks correlates with the amount of RH414 T-tubule RH414 staining found at the A-band.

Electron Microscopy

Muscles from WT, *Dysf*, MKO, and FER mice were dissected and placed in 4% paraformaldehyde. Muscles were fixed in 2.5% glutaraldehyde, post-fixed in 1% OsO_4 for 1hour at 4°C, rinsed, dehydrated in ethanol, and infiltrated overnight. Embedded samples were divided into sections and stained with 1% uranyl acetate, followed by

lead citrate. For T-tubule staining, muscles were fixed in glutaraldehyde overnight, post-fixed in 2% osmium tetroxide containing 0.8% potassium ferrocyanide for 1 hour at room temperature, and processed as previously described.[16]

Tubular Aggregate Quantification

Quadricep muscles from male and female 6-month-old WT, *Dysf*, MKO, and FER mice were prepared for electron microscopy analysis, as previously described. Tubular aggregates within myofibers were counted in at least 12 grid squares per animal, with each grid containing approximately 8 to 12 fibers. At least three animals were analyzed per genotype. Muscles from 6-month-old animals were stained with anti-dystrophin and anti-SERCA1, and imaged under immunofluorescence microscopy. SERCA1-positive aggregates were counted from >85 fibers and four samples per genotype.

Oil Red O

Quadricep muscles were divided into sections, rinsed with PBS, and then fixed with 10% formalin. Samples were rinsed, dehydrated with 60% isopropanol, and air dried. Lipids were stained with oil red O for 10 minutes, rinsed, and fixed. Images were captured using a Zeiss Axiophot microscope. Primary myoblasts, isolated similar to the methods described for neonatal WT, *Dysf*, MKO, and FER mice, were stained as previously described.[22] Lipid droplets were quantified from 75 myoblasts per genotype.

MRI and Quantification

Nine-month-old WT, *Dysf*, *MKO*, *FER* mice, two males and two females of each genotype, were imaged at the University of Florida (Gainesville). Magnetic resonance imaging (MRI) was performed in a 4.7-T horizontal bore magnet (Varian, Palo Alto, CA). The animals were anesthetized using 0.8 to 1 L/minute oxygen and isoflurane mixture (3% isoflurane) and maintained under 0.5% to 1% isoflurane for the duration of the MR procedure. Body temperature was maintained through an MR-compatible heating system that pumped heated air into the bore of the magnet, and respiratory rate was monitored for the duration of the scans (Small Animal Instruments, Inc., Stony Brook, NY). The hind limbs of each mouse were inserted into a custom-built solenoid ^{1}H-coil (200 MHz) with a 2.0-cm internal diameter. Three-dimensional spin-echo images were acquired with the following parameters: repetition time, 1000 milliseconds; echo time, 20 milliseconds; echo train length, 8; matrix size, 192 × 192 × 128; field of view, 20 × 20 mm^2. T_1-weighted images were acquired using series of repetition times (6, 3, 2, 1, 0.5, and 0.25 seconds): echo time, 5.7 milliseconds; matrix size, 128 × 128; field of view, 20 × 20 mm^2; number of slices, 4; slice thickness, 1.00 mm with gap of 1 mm. Mutliplanar MR images acquired from both hind limbs were converted to Digital Imaging and Communications on Medicine format using a custom-written IDL code for Varian data (ITT Visual Information Systems, Boulder, CO); subsequent regions of interest were measured with Osirix (Pixmeo, Geneva, Switzerland). Fatty tissue deposition behind the knee joint (popliteal fossa) was outlined on multiple images, and the volume of fatty tissue deposition was calculated based on these regions of interest.

Statistical Analysis

Statistical analyses were conducted with Prism using an unpaired *t*-test, unless otherwise noted.

Results

Severe Disease Pathological Features in FER Muscle

The naturally occurring dysferlin-null allele arose in the A/J mouse line housed in the Jackson Laboratory (Bar Harbor, ME) through a retrotransposon insertion into intron 4 of the dysferlin locus.[25] We previously bred this allele into the 129/SV emst/J line through six successive generations to generate the dysferlin-null allele in the 129S/V emst/J background (referred to as *Dysf*).[1] This *Dysf* allele was crossed onto the 129/SV emst/J line carrying the myoferlin-null mutation (*MKO*) to generate a dysferlin-myoferlin double-null ferlin mouse line.[20] FER mice are viable and can survive to >100 weeks (data not shown), despite myoferlin and dysferlin both having a high level of expression in the heart.[18] We examined multiple muscle groups from older animals (aged 14 months), because these muscle groups at this age are most likely to show pathological features in *Dysf* mice. FER muscle consistently showed enhanced pathological features, with more evident immune infiltrate, fatty infiltrate, greater fiber splitting, increased fiber size variability, and internalized nuclei (n = 3 for each genotype) (Figure 1A). *Dysf* muscle had similar dystrophic features, but to a lesser degree, than what was seen in FER muscle. *MKO* muscles, even in older animals, had few areas of immune or fatty infiltrate and only rare internalized nuclei. *MKO* animals were more reminiscent of WT controls, which showed no dystrophic changes.

Creatine kinase (CK), a highly expressed enzyme in brain, skeletal muscle, and heart, is released after trauma or with membrane disruption. Clinically, this increase of serum CK is used as an indicator of muscle damage. Serum CK levels were assessed from 14-month-old, WT, myoferlin-null, dysferlin-null, and FER mice (n = 12, 9, 8, and 11, respectively). Figure 1B shows the markedly elevated CK levels of *Dysf* and FER mice. CK levels in WT (209 U/L) and myoferlin-null (180 U/L) mice were similar, whereas the mean serum CK in *Dysf* (1117 U/L) was elevated five-fold. FER CK was higher than that of *Dysf* (1880 U/L).

Muscles from younger (24-week) WT, *MKO*, *Dysf*, and FER mice also showed enhanced pathological features in

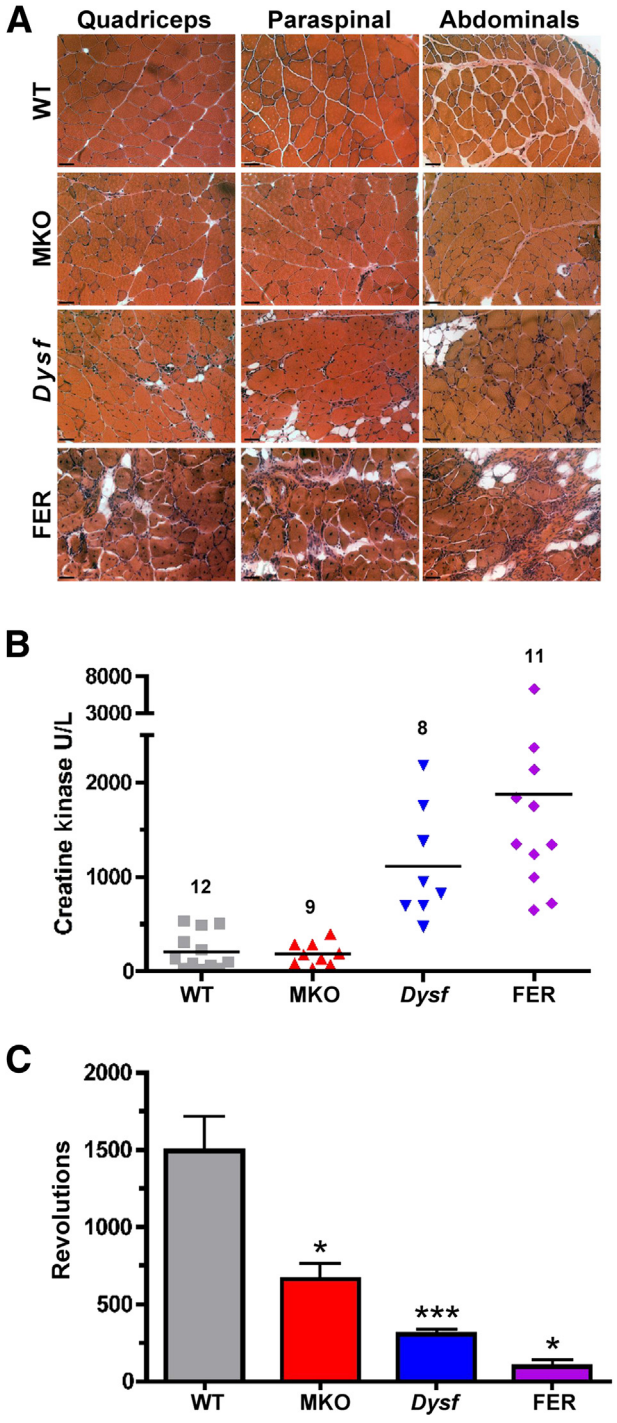

Figure 1 Severe muscle disease in FER mice. **A**: Representative H&E images from 14-month-old wild-type (WT), mice lacking myoferlin (*MKO*), *Dysf*, and mice lacking both myoferlin and dysferlin (FER) quadricep, paraspinal, and abdominal muscles stained with H&E. *Dysf* and FER muscles display characteristic features of muscular dystrophy, including internalized nuclei, fibrosis, fiber splitting, necrosis, fat, and immune infiltrate. In all muscle groups, the FER muscles showed the most severe pathological characteristics. **B**: Distribution plot of creatine kinase (CK) values from 14-month-old WT, *MKO*, *Dysf*, and FER mice showing increased CK levels in FER mice. **C**: The 16-month-old FER mice are the least active of all strains represented by a decrease in the mean number of wheel revolutions during free exercise. $*P < 0.01$, $***P < 0.0001$. Scale bar = 20 μm (**A**).

FER mice (Supplemental Figure S1A). The mean cross-sectional area of both FER (8453 μm^2) and dysferlin-null (8511 μm^2) mice was reduced compared with WT mice (9371 μm^2) ($P = 0.036$ and $P = 0.015$, respectively) (Supplemental Figure S1B). This decrease was more pronounced than the loss of myoferlin alone (8990 μm^2). In addition, FER quadricep muscles had the greatest percentage of fibers containing internalized nuclei (Supplemental Figure S1C), at 24%, compared with dysferlin-null quadriceps containing 13%, and myoferlin-null and WT muscle each containing 1% ($P < 0.005$ for all comparisons, except WT versus *MKO*, which was nonsignificant) ($n = 3$ mice per genotype; $n > 2000$ fibers) (Supplemental Figure S1D).

Decreased Activity in Ferlin-Null Mice

To evaluate muscle activity, 16-month-old mice were allowed free access to a running wheel and monitored for 48 hours. Wheel activity was analyzed from 5 p.m. to 5 a.m., a time period when mice are most active. *MKO*, *Dysf*, and FER mice all ran significantly less than WT mice (665, 309, 93, and 1695 mean revolutions per night, respectively) (Figure 1C). These data are consistent with the histopathological findings and suggest functional deficits similar to what occurs in human patients with dysferlinopathy. Furthermore, the loss of myoferlin on its own elicits far less phenotype, but when in the context of the *Dysf*-null allele, it exacerbates the dystrophy process both pathologically and functionally.

Progressive Muscular Dystrophy in FER Mice

The cyclic pathway of muscle degeneration and regeneration in dystrophic muscle is characterized by a variety of histological factors, including increased fatty and immune infiltrate and the internalization of myofiber nuclei. The internalization of muscle nuclei is a sign of ongoing repair after myofiber damage. In progressive forms of dystrophy, increasing numbers of myofibers degenerate over time, outpacing repair. To determine whether FER mice display progressive muscular dystrophy, we evaluated the onset and progression of dystrophic pathological characteristics (Supplemental Figure S2A). At 2 months of age, FER muscle contained mild dystrophic changes, observing only a few internalized nuclei. At 6 months of age, the abdominal and paraspinal muscles were the most affected muscle groups, showing fibro-fatty-immune infiltrate and fiber necrosis. At 14 months of age, the FER-null mice had severe signs of muscular dystrophy. All five muscle groups, except the gastrocnemius/soleus, showed internalized nuclei, fiber splitting, fibro-fatty changes, immune infiltrate, and variable fiber size. At this time point, the abdominal and paraspinal muscles remained the most severely affected muscle groups, followed by the gluteus/hamstring, quadriceps muscle, triceps, and gastrocnemius/soleus ($n = 3$ for each age group and muscle analyzed). The WT mice did not show features

of dystrophy in any muscle group analyzed at any age (data not shown). Correlating with the histological data, FER serum CK levels progressively increased from 2 months (404 U/L) to 6 months (556 U/L) up to 14 months (1762 U/L) of age. FER CK levels were significantly higher than in WT controls at 2 months (100 U/L, $P = 0.01$), 6 months (98 U/L, $P = 0.05$), and 14 months (217 U/L, $P = 0.001$) (Supplemental Figure S2B).

Lipid Accumulation and Extrusion from FER Muscle

FER muscle displayed a marked fatty infiltrate (Figure 1 and Supplemental Figure S2), which is typically seen as adipocytes in between myofibers, but can also can be present as grossly evident fatty accumulation. MRI was performed of hindquarters from 9-month-old *MKO*, *Dysf*, and FER mice, which contained visible fatty accumulation ($n = 4$ mice per genotype) (Figure 2A). The volume of fat accumulation from the MRI images was quantified, and *MKO*, *Dysf*, and FER muscle contained significantly more fat in the hind limbs than in WT controls ($P < 0.01$ and $P < 0.001$, $n = 4$ mice per genotype) (Figure 2B). By using oil red O, a fat-soluble dye that stains neutral lipids, muscle from *MKO*, *Dysf*, and FER was noted to have large and small lipid droplets within the myofibers qualitatively more than normal muscle (Figure 2C). Furthermore, lipid droplets appeared to exude from ferlin-mutant muscle, especially FER muscle, whereas this same phenomenon was only rarely seen in WT (Figure 2D). A representative image demonstrates the membranous neck between the body of the lipid droplet and the muscle membrane, indicating that these droplets are contiguous with the muscle membrane. Lipid droplet formation was quantified in muscle precursor cells, myoblasts. *Dysf* and FER myoblasts contained significantly more oil red O−positive lipid droplets than WT controls ($P < 0.0001$, $n >$ 75 myoblasts) (Supplemental Figure S3). The content of these vesicles is unknown, but in Figure 2E, we measured the serum content of glycerol, from 14-month-old mice, and found it increased in FER mice (4.33 mg/dL) compared with WT controls (3.1 mg/dL) ($P = 0.02$, $n > 5$ mice per genotype). Serum glycerol was not increased in myoferlin-null (2.97 mg/dL) or dysferlin-null (3.946 mg/dL) mice compared with WT, but the values were trending toward significance for dysferlin ($P = 0.065$).

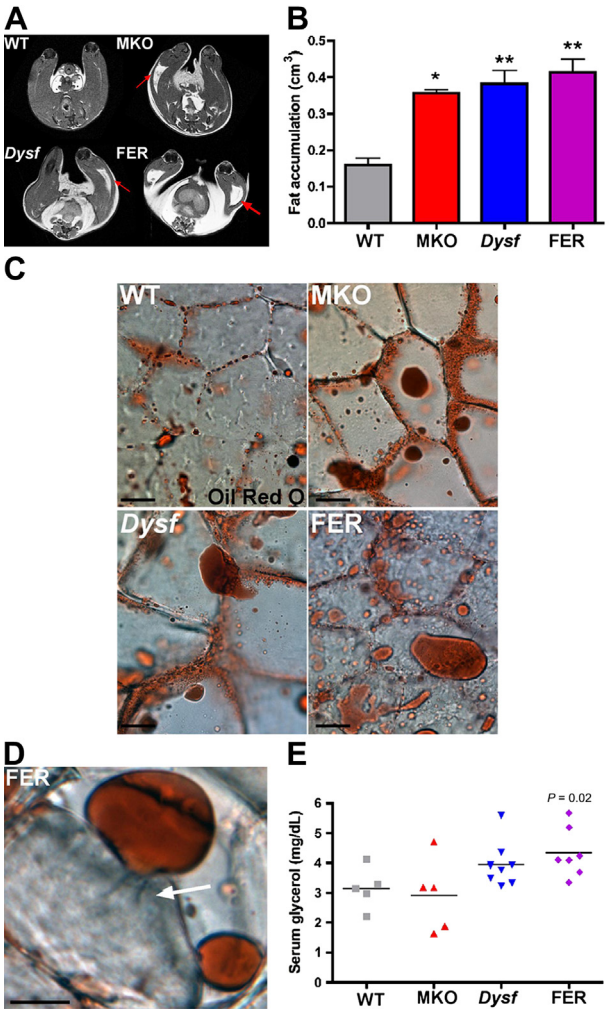

Figure 2 Lipid accumulation in skeletal muscel of mice lacking both myoferlin and dysferlin (FER). **A:** MRIs show fat accumulation in mice lacking myoferlin (*MKO*), *Dysf*, and, most substantially, FER hind limbs (**red arrows**). **B:** Increased fat accumulation in MKO, *Dysf*, and FER hind limbs by MRI. $*P < 0.01$, $**P < 0.001$. **C:** Wild-type (WT), MKO, *Dysf*, and FER quadriceps muscle was stained with oil red O to label lipids within the muscle. Representative images are shown. MKO, *Dysf*, and FER muscles contain visibly more increased oil red O lipid staining than WT. **D:** A high-magnification image of an extruding lipid droplet from FER muscle is shown (**white arrow**). **E:** Serum glycerol levels are elevated in 14-month-old FER serum. Scale bar = 10 μm (**C** and **D**).

Progressive Sarcotubular Abnormalities in FER Muscle

T-tubules abut the sarcoplasmic reticulum (SR) to form triads, a unit that promotes coordinated coupling between excitation and contraction. Electron microscopy shows that triads are present in FER muscle (Figure 3A). Calcium-potassium ferrocyanide staining was applied to visualize specifically the T-tubules in these young (8-week-old) muscles, highlighting that FER T-tubules were elongated compared with those in WT (Figure 3A). Vacuolated structures were also present within FER muscle at this time point (8 weeks), which appears to be dilated SR but may also include T-tubules. By 6 months of age, large vacuolated sarcotubules become prominent (Figure 3B). Because T-tubules undergo turnover, we hypothesize that sarcotubule defects in FER muscle represent the accumulation of excess membrane arising from decreased vesicle trafficking/recycling.[1,21,22]

We compared the ultrastructure among the different genotypes. Electron microscopy of 6-month-old quadriceps muscle demonstrated intact triad structures in all genotypes (Figure 4A). FER muscle had the most severe sarcotubule defects compared with *MKO*, *Dysf*, and WT, with areas of disorganization and SR dilation (Figure 4A). Tubular aggregates are densely packed membrane abnormalities believed to originate from the sarcoplasmic reticulum and

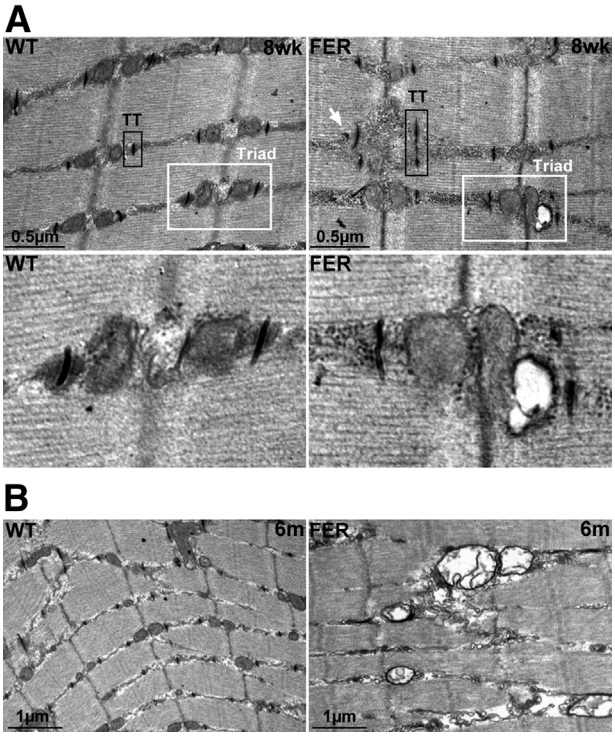

Figure 3 Progressive sarcotubular abnormalities in skeletal muscle of mice lacking both myoferlin and dysferlin (FER). **A:** Representative electron microscopy images from young (8-week-old) wild-type (WT) and FER quadriceps muscle stained with potassium ferrocyanide, which stains T-tubules. FER muscle contains elongated T-tubules (TTs) highlighted by **black boxes**. A **white arrow** highlights ectopic T-tubule formation in FER muscle. **White boxes** highlight a triad that is magnified (**bottom panels**). FER muscle contains vacuolated, malformed T-tubules. **B:** Progressive mislocalization, elongation, and vacuolation of T-tubules and dilation of the sarcoplasmic reticulum in older FER muscle (6 months old).

form in a variety of muscle disorders, including periodic paralysis, myotonia congenita, myalgia, and myasthenic myopathy.[28–30] Tubular aggregates were found in all genotypes, except WT, in a variety of sizes and locations within the myofiber (Supplemental Figure S4). A high-magnification image of a tubular aggregate in an FER fiber depicts the dense packing of the aggregate in the characteristic honeycomb pattern (Figure 4B).[31] Tubular aggregates were present in approximately 15% of the FER myofibers, whereas MKO and *Dysf* fibers had fewer (4% and 2%, respectively). All genotypes contained more aggregates than WT controls (0.1%, $P < 0.005$ for all comparisons) (Figure 4C).

Tubular aggregates are composed of multiple proteins, including the SR proteins, the SERCA1.[29] The tubular aggregates in these mutants were SERCA1^{+}, with FER fibers showing large and frequent SERCA1^{+} tubular aggregates (Figure 5A), whereas WT muscle had none of these aggregates. FER fibers contained 21.9% SERCA1^{+} fibers, whereas *Dysf*, MKO, and WT contained significantly fewer aggregates, similar to the results obtained in the electron microscopy analysis. We imaged the DHPR receptor, a T-tubule protein, using immunofluorescence microscopy in 6-month-old FER FDB. As seen by electron microscopy, the DHPR staining was disorganized and ectopic in FER FDB fibers, whereas a normal organized DHPR pattern was seen in WT FDB fibers (Figure 5C). In addition, immunoblotting of WT and FER quadriceps muscle showed increased protein levels of annexin A2, Fer1L5, and DHPR in FER muscles compared with WT at 6 months. Interestingly, caveolin-3 expression was decreased in FER muscle.

Ferlin T-Tubules Are More Susceptible to Glycerol-Induced Damage

T-tubules are approximately 80% of muscle membrane and contribute significantly to the regulation of muscle osmolarity.[32] Acute glycerol exposure and then withdrawal induces osmotic shock, resulting in separation of the T-tubule from the SR and disruption of excitation-contraction coupling within the fiber.[27,33–35] Transient glycerol exposure triggers T-tubules to lose continuity with the sarcolemma and pinch off, forming intracellular vacuoles; it also disrupts the proximity of the T-tubule and SR.[36] This process of detubulation or vacuolization is reversible on restoration of normal osmotic pressure, consistent with the dynamic nature of T-tubules (Figure 6A). We isolated FDB fibers from 8-week-old WT and FER muscle and loaded the fibers with RH414, a potentiometric dye that anchors itself

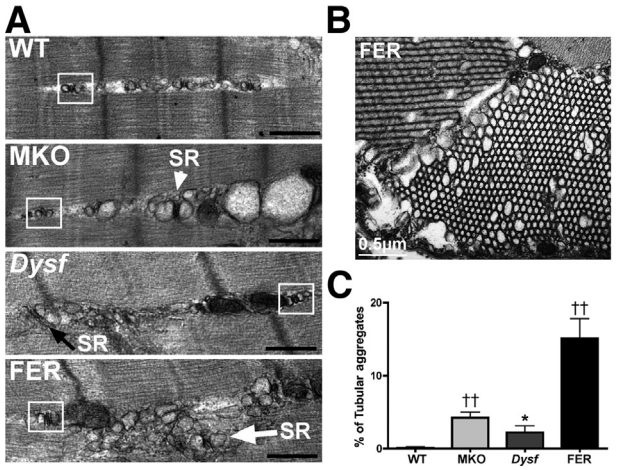

Figure 4 Sarcotubular defects in *Dysf*, mice lacking myoferlin (*MKO*), and mice lacking both myoferlin and dysferlin (FER) muscle. **A:** Representative electron microscopy images from 6-month-old wild-type (WT), *MKO*, *Dysf*, and FER quadriceps muscle. A **white box** depicts intact triads in WT, *MKO*, and *Dysf* muscles. SR dilation highlighted in *MKO* muscle (**white arrowhead**). A **black arrow** shows elongated and semidilated SR in *Dysf* muscle. FER myofibers were the most abnormal, frequently showing complete sarcotubule disorganization characterized by T-tubule elongation, SR dilation, and ectopic triad formation over A-bands (**white arrow**). **B:** High-magnification image of a characteristic tubular aggregate found in the FER muscle. **C:** Tubular aggregates were increased in *MKO*, *Dysf*, and FER quadriceps compared with WT, with FER muscle showing nearly 15% of fibers with tubular aggregates. *$P < 0.005$, *Dysf* to WT; $^{\dagger\dagger}P < 0.001$, MKO and FER to WT.

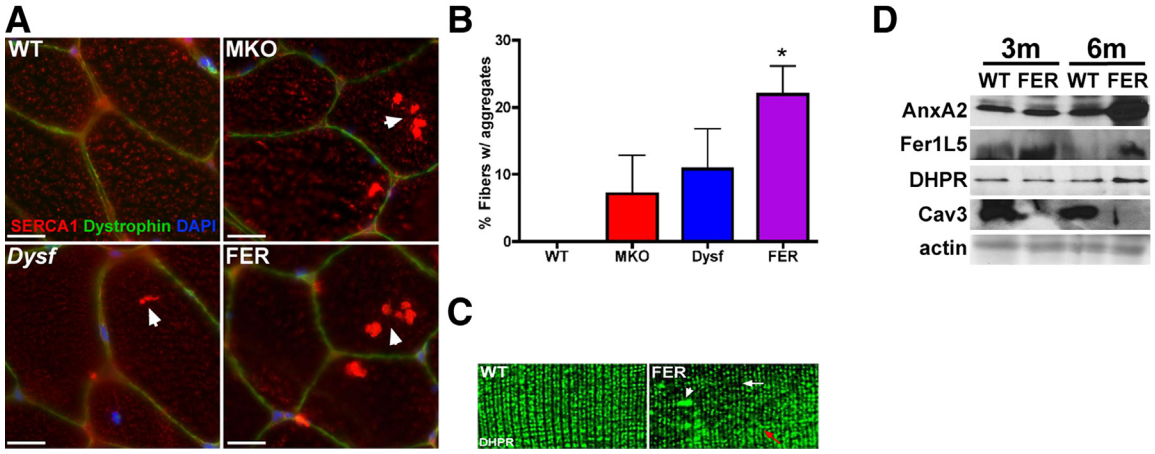

Figure 5 Abnormal SR and T-tubule staining in muscle in mice lacking both myoferlin and dysferlin (FER). **A:** Representative images showing abnormal SERCA1-positive aggregates illustrated by the presence of anti-SERCA1 (red) staining within the mice lacking myoferlin (*MKO*), *Dysf*, and FER myofibers defined by the anti-dystrophin (green) outline. No SERCA1^{+} aggregates were seen in wild-type (WT) muscle. Nuclei are stained with DAPI (blue). Scale bar = 20 μm. **B:** SERCA1^{+} aggregates were increased in FER quadriceps myofibers compared with WT. *$P < 0.002$. **C:** Representative images showing anti-DHPR (green) staining. Areas of DHPR staining are diminished (**white arrow**), disorganized (**red arrow**), and ectopically overexpressed (**white arrowhead**) in FER flexor digitorum brevis (FDB) fibers compared with the ordered DHPR staining pattern in WT FDB fibers. **D:** Immunoblotting of muscle lysates from 3- and 6-month-old WT and FER mice. Protein levels of annexin 2, Fer1L5, and DHPR are elevated in FER muscle at 6 months, whereas caveolin-3 is decreased. Actin is shown as a loading control.

in the lipid bilayer at the T-tubule.[27] Glycerol exposure also induces shrinkage, or crenation, which on glycerol removal is followed by a volumetric increase in the early phase of recovery from glycerol-induced osmotic shock (Figure 6A). In FDB fibers, this can be measured as the myofibers transiently increase their volume for 1 minute after removal of glycerol. After this, fibers return to close to normal size. In contrast to WT, FER fibers failed to increase in size after glycerol removal (Figure 6B). In addition, FER fibers remained smaller than WT fibers from 1 to 15 minutes ($P < 0.04$). Fiber size was normalized to the fiber size at time 0 minutes to mark change in fiber size during the recovery period. The normalized fiber size at time 1 minute into recovery was plotted in Figure 6C.

Normal FDB fibers displayed a brief vacuolization of the T-tubule and then recovery, indicating the normal recovery after osmotic shock (Figure 7A). In contrast, during recovery from osmotic shock, FER T-tubules formed large visible vacuoles, which persisted over the 15-minute time course (Figure 7A). Both *MKO* and *Dysf* FDB fibers also displayed abnormal recovery from glycerol-induced osmotic shock. *MKO* fibers demonstrated aggregated T-tubules, whereas *Dysf* fibers had T-tubule vacuolation persisting 15 minutes into recovery. The pattern in *Dysf* fibers was similar to, but not always as pronounced as in, FER myofibers (Supplemental Movies S1, S2, S3, and S4). Interestingly, mutant fibers at baseline appeared to have decreased levels of RH414 signal at the T-tubule, suggesting a potential decrease in membrane potential or altered lipid bilayers that bind less RH414.

To compare the T-tubule organization between WT, MKO, *Dysf*, and FER fibers, fast-Fourier transformation (FFT) was performed at time 0 and 15 minutes after glycerol withdrawal using the RH414 signal (Figure 7B). Normally, T-tubules found in a periodic organization manifest as peaks in the FFT power spectrum. When T-tubules are absent or disrupted, this regularity is lost and the peak power amplitude is decreased. Periodic spacing was noted in WT fibers,

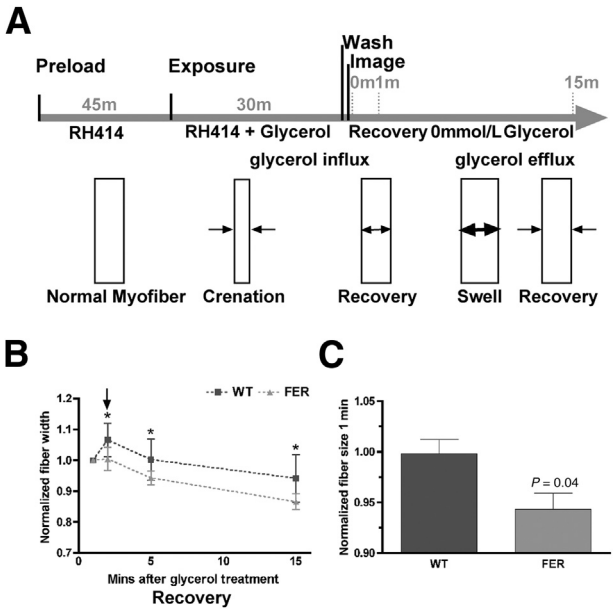

Figure 6 Fibers in mice lacking both myoferlin and dysferlin (FER) do not dilate in response to glycerol-induced osmotic shock. **A:** A scheme representing the normal myofiber response to osmotic shock induced by transient glycerol exposure. **B:** At 1 minute after glycerol removal (**arrow**), normal fibers swell, reflecting osmotic pressure. After this, the fiber recovers. In contrast, FER fibers do not swell and then shrink further during the recovery phase. *$P < 0.05$. **C:** Normalized FER flexor digitorum brevis (FDB) fibers are smaller than wild-type (WT) fibers at 1 minute after glycerol removal.

with two dominant peaks at 0.5 and 1 μm at time 0. The addition of glycerol caused a slight reduction in peak power because the organization of the T-tubules remained generally intact. MKO fibers at time 0 show similar periodicity to WT fibers, with peaks noted at 0.5 and 1 μm. However, by 15 minutes after glycerol treatment, MKO fibers lose T-tubule organization, becoming aggregated, as seen by the loss of the secondary peak at 1 μm. FFT analysis revealed major defects in T-tubule organization in both *Dysf* and FER fibers. *Dysf* fibers show mild periodicity because T-tubules are not organized at both time 0 and 15 minutes after glycerol withdrawal. FER fibers only show one dominant peak at time 0 at 1 μm, correlating with the difference in spacing of the RH414 signal in Figure 7A. At 15 minutes after glycerol withdrawal, FER fibers lose peak power at 1 μm because T-tubule organization is lost. These data demonstrate that MKO, *Dysf*, and FER T-tubules are structurally defective, especially in the face of osmotic shock induced by glycerol.

Glycerol-Induced *in Vivo* Damage Recapitulates Dystrophy in FER Mice

Direct glycerol injection into muscle induces myopathic pathological characteristics with a pronounced adipocyte infiltration.[26] We tested the susceptibility of young (8-week-old) FER muscle to glycerol-induced myopathy and compared it with WT by directly injecting the tibialis anterior muscle with 50% glycerol. Mice were examined 28 days after injection to allow adequate time for regeneration and recovery. Figure 8A shows that WT muscle, 28 days after glycerol injection, had regenerated well. The central portion of the fiber reflects the injection site, which likely retained some adipocyte infiltration that cleared with fixation. Notably, the myonuclei near this area were internally located, indicating recent regeneration. FER muscle remained highly infiltrated with adipocytes at this same time point, with evidence of adipocyte infiltration extending substantially beyond the injection site. Glycerol-injected FER muscle had many internally nucleated fibers indicative of ongoing regeneration. These characteristics are reminiscent of those seen in aged, diseased FER muscle (Figures 1 and 2). Injection of a 1% glycerol solution yielded similar results (Supplemental Figure S5A). In addition, the injection of serum from 14-month-old aged FER mice was sufficient to induce fiber damage in young 2-month-old FER muscle but not WT muscle. Because old FER mice contain elevated glycerol (Figure 3), we hypothesize that the glycerol content in FER muscle is sufficient to induce damage in a feed-forward mechanism. At 5 days after injection, FER muscle showed internalized nuclei, fatty infiltrate, and immune infiltrate, whereas WT TA muscle remained uninjured (Supplemental Figure S5B).

In Vivo Glycerol-Induced Sensitivity in MKO, *Dysf*, and FER Muscle

We next tested the sensitivity of young 2-month-old *MKO*, *Dysf*, and FER muscle to glycerol-induced myopathy. The tibialis anterior muscle was injected with 50% glycerol and

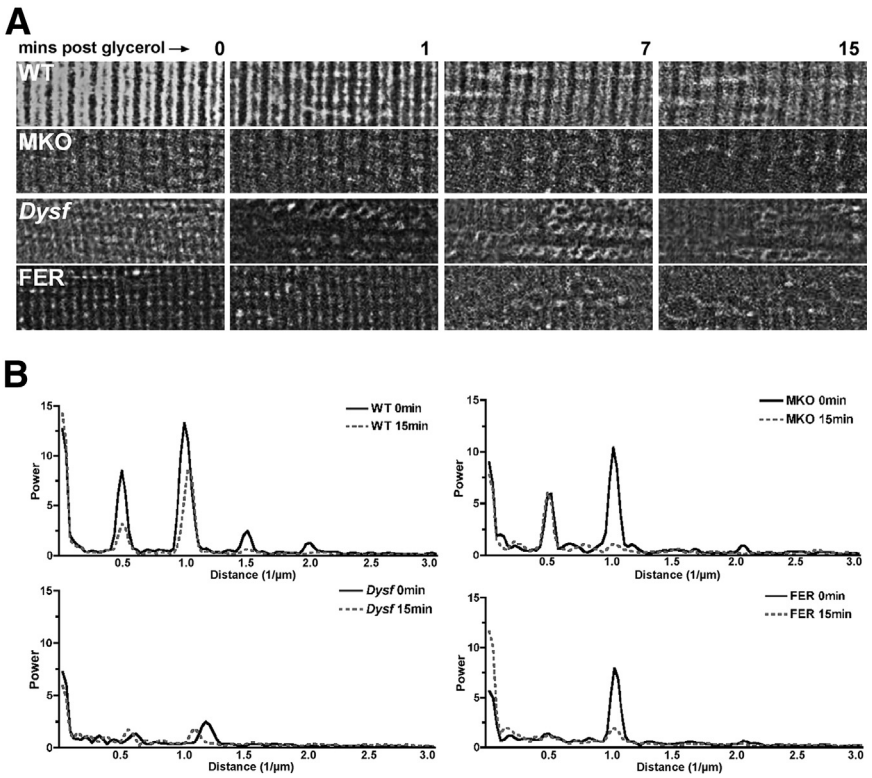

Figure 7 Abnormal and persistent dilation of T-tubules in mice lacking both myoferlin and dysferlin (FER) after glycerol-induced hyperosmotic shock. **A**: Flexor digitorum brevis (FDB) fibers during recovery after glycerol exposure. Images were acquired at 0, 1, 7, and 15 minutes after glycerol removal. Wild-type (WT) fibers lose some RH414 fluorescence at 7 and 15 minutes. In contrast, *Dysf* and FER T-tubules vacuolate by 1 minute, and this vacuolization persists throughout recovery. In mice lacking myoferlin (*MKO*) T-tubules have reduced RH414 intensity and aggregate during recovery from glycerol. **B**: Fast-Fourier transforms were conducted on images during recovery from glycerol. Profiles are shown for all four genotypes (WT, MKO, *Dysf*, and FER). The two lines in each profile represent the data from at the beginning of imaging (time 0) and at 15 minutes of imaging (15 minutes). With this analysis, *Dysf* and FER appeared the most distinct from WT, with reduced power peaks, and, in the case of FER, only a single peak.

examined 28 days after injection to allow the muscle sufficient time for repair. Supplemental Figure S6 shows that *MKO*, *Dysf*, and FER muscle displayed an increased sensitivity compared with WT controls. WT muscle has relatively few fibers containing internal nuclei, and low levels of immune or fatty infiltrate. *MKO*, *Dysf*, and FER all contain myofibers with internalized nuclei and muscles with increasing levels of inflammation and fatty infiltrate. These data are consistent with a model of heightened sensitivity to T-tubule vacuolation *in vivo* and an inability to recover from glycerol-induced myopathy.

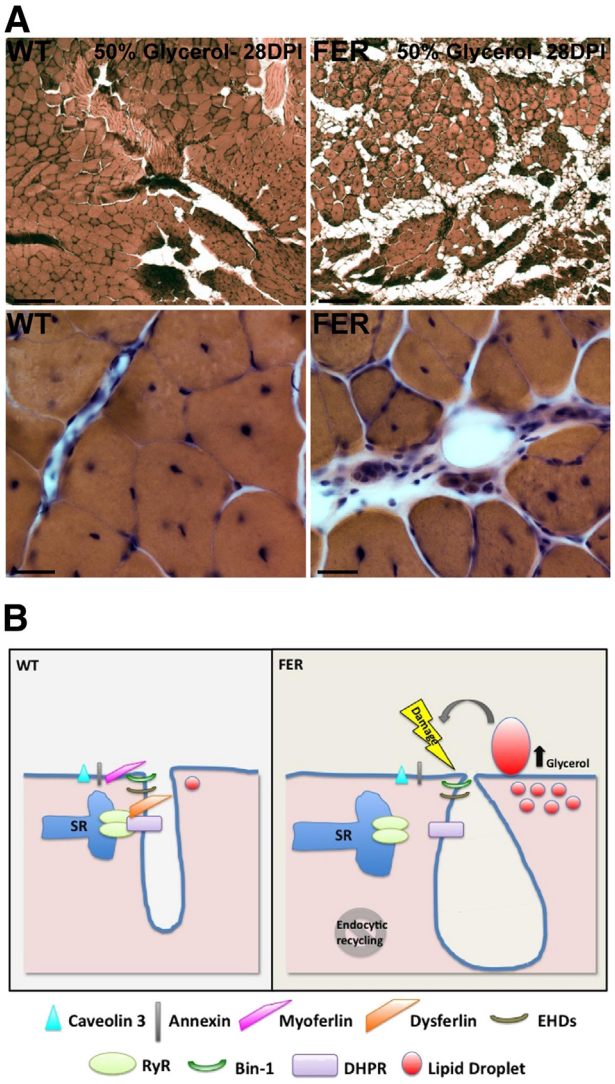

Figure 8 Increased *in vivo* glycerol sensitivity in mice lacking both myoferlin and dysferlin (FER) muscle. **A**: Glycerol was injected into the TA muscle of 2-month-old wild-type (WT) and FER muscle. After a 28-day recovery period, tissue was harvested and stained with H&E. Low-magnification images (**top panels**) and high-magnification images (**bottom panels**). Scale bar = 10 μm. Glycerol was sufficient to induce a dystrophic phenotype in 2-month-old FER animals, reminiscent of that seen in 14-month-old FER animals, including central nuclei, fat accumulation, fiber splitting, immune infiltration, and fiber size variability. **B**: Model for defective T-tubule formation and function in FER mice. In WT muscle, dysferlin, caveolin-3, Bin-1, and the EHD proteins associate at the T-tubule. Defects in membrane trafficking caused by the loss of myoferlin and dysferlin in ferlin-null muscle produces an accumulation of lipids, which exude from the membrane, producing a local increase in extramyofiber lipid concentration. With injury or osmotic shock induced from increased local lipid concentrations, FER T-tubules become vacuolated, contributing to muscle weakness through defective excitation-contraction coupling. Long-term adipocyte infiltration into dysferlin dystrophic muscle further increases local lipid concentration, thereby promoting additional vacuolation.

Discussion

Limb-girdle muscular dystrophy type 2B, Miyoshi myopathy, and distal anterior compartment myopathy result from disruption of the *DYSF* gene. The exact role of dysferlin and how it mediates these variable muscle-related phenotypes are unknown. The comparatively mild phenotype in multiple *Dysf* mouse models has hampered progress in dissecting dysferlin's role. We generated mice lacking both myoferlin and dysferlin (FER), finding an enhanced phenotype that points to T-tubule formation and function as a key component of the mechanism by which dysferlin loss leads to muscle destruction. Myoferlin is homologous to dysferlin, but differs slightly in its expression pattern. Although dysferlin is expressed at low levels in myoblasts and increases its expression in mature myofibers, myoferlin is expressed at higher levels in myoblasts, especially those poised to fuse, and then is down-regulated in mature myofibers. Myoferlin expression is triggered by muscle damage. For example, *MKO* muscle injected with cardiotoxin, a standard approach to induce muscle damage, recovers poorly and, instead, displays features of dystrophy after injury, consistent with impaired degeneration. Myoferlin is expressed at low levels in mature myofibers, where its expression is membrane associated, including the internalized membrane structures, such as the perinuclear endoplasmic reticulum and plasma membrane. We hypothesize that a major aspect of the FER muscle's enhanced pathological features derives from impaired regeneration from loss of myoferlin and, specifically, its role in myoblast fusion.

Enhanced adipocyte infiltration into muscle occurs in several muscle disorders, including muscular dystrophy. However, the degree of fatty infiltration in different forms of muscular dystrophy varies with subtype and mutation. We hypothesize that the increase in lipid droplets in *MKO*, *Dysf*, and FER muscle may derive from defective membrane trafficking and processing. Zhang et al[37] previously used mass spectrometry to evaluate the protein content of muscle-derived lipid droplets, finding myoferlin, dysferlin, and EHD family members. FER mice developed a progressive, fatty infiltration, with adipocytes found between myofibers and excessive lipid accumulation within and exuding from myofibers. In addition, serum glycerol was elevated in FER animals. Intramuscular glycerol injections have been shown previously to increase fatty deposition in skeletal muscle and to result in muscle damage.[26] Therefore, we hypothesize that neutral lipids, including glycerol, are increased in dysferlinopathy, which, in

turn, promotes *in vivo* detubulation and osmotic shock to neighboring myofibers.

Dysferlin at the T-Tubule

Dysferlin is a membrane-associated protein, and *Dysf* muscle does not reseal efficiently after laser-induced disruption of the plasma membrane.[2] These findings do not preclude additional roles for dysferlin in the muscle. Dysferlin was found at the T-tubule in developing and mature muscle.[15] To further explore sarcotubular uncoupling in detail, we used a well-established method of glycerol exposure.[27,38,39] *Ex vivo*, we found glycerol is sufficient to vacuolate T-tubules in young FER FDB fibers, suggesting heightened sensitivity of FER fibers. This increased sensitivity of FER fibers is presumed to be a consequence of the elongated and irregular T-tubules, and the structural abnormalities precede the histopathological changes. *In vivo*, we found glycerol-induced T-tubule damage in young animals is sufficient to recapitulate the 14-month dystrophic phenotype, including myofiber splitting, internalization of nuclei, and fibro-fatty-immune infiltrate.

We propose a model in which ferlin proteins, primarily dysferlin and, to a lesser extent, myoferlin, along with interacting partners, such as caveolin-3, Bin-1, and the EHDs, are present at the sarcolemma. On insult, the annexins, Bin-1, dysferlin, EHDs, and caveolin-3, are increased at the T-tubule to induce repair.[15–17,40] In this model (Figure 8B), the lack of functional ferlins and reduced vesicle trafficking result in increasing accumulation of myofiber lipids.[1,22] In the absence of functional ferlins, the T-tubule and plasma membrane are unable to be repaired, resulting in the release of lipids, including glycerol. The local increase in lipid content, including glycerol, further promotes myopathy by functionally separating the T-tubule from the sarcolemma and SR. The environment surrounding the injured fibers ultimately promotes adipogenesis.[41] Once adipocytes accumulate within the muscle, more glycerol is generated within the muscle through lipolysis.[42] This generates an additional source of glycerol available to damage the sarcotubule system. The increase in adipocyte infiltration in this model is expected to contribute to the progressive dystrophic phenotype.

Over time, these defects may eventually result in the formation of nonfunctional triads and altered calcium homeostasis, further enhancing muscle weakness. Defects in triad formation leading to muscle weakness and excitation contraction coupling have been documented in other mutant mice, including mitsugumin-29 and junctophilin 1, proteins that localize to the sarcotubule network.[43–45] Of interest, the junctophilin 1, 2 double-mutant muscle also contains stacks of SR, similar to the tubular aggregates found in FER muscle. This model supports additional roles for myoferlin and dysferlin, in using trafficking and fusogenic properties beyond sarcolemmal repair in the biogenesis and maintenance of the sarcotubular system in skeletal muscle; the model would help explain the failure of myoferlin to compensate for the loss of dysferlin *in vivo* in mice.[46] We propose that alterations in the T-tubule and triad are a primary cause of weakness in dysferlinopathy, and these data suggest a new avenue for therapeutic targets.

Supplemental Data

Supplemental material for this article can be found at *http://dx.doi.org/10.1016/j.ajpath.2013.09.009*.

References

1. Demonbreun AR, Fahrenbach JP, Deveaux K, Earley JU, Pytel P, McNally EM: Impaired muscle growth and response to insulin-like growth factor 1 in dysferlin-mediated muscular dystrophy. Hum Mol Genet 2011, 20:779–789
2. Bansal D, Miyake K, Vogel SS, Groh S, Chen CC, Williamson R, McNeil PL, Campbell KP: Defective membrane repair in dysferlin-deficient muscular dystrophy. Nature 2003, 423:168–172
3. Liu J, Aoki M, Illa I, Wu C, Fardeau M, Angelini C, Serrano C, Urtizberea JA, Hentati F, Hamida MB, Bohlega S, Culper EJ, Amato AA, Bossie K, Oeltjen J, Bejaoui K, McKenna-Yasek D, Hosler BA, Schurr E, Arahata K, de Jong PJ, Brown RH Jr.: Dysferlin, a novel skeletal muscle gene, is mutated in Miyoshi myopathy and limb girdle muscular dystrophy. Nat Genet 1998, 20:31–36
4. Saito H, Suzuki N, Ishiguro H, Hirota K, Itoyama Y, Takahashi T, Aoki M: Distal anterior compartment myopathy with early ankle contractures. Muscle Nerve 2007, 36:525–527
5. Bashir R, Britton S, Strachan T, Keers S, Vafiadaki E, Lako M, Richard I, Marchand S, Bourg N, Argov Z, Sadeh M, Mahjneh I, Marconi G, Passos-Bueno MR, Moreira Ede S, Zatz M, Beckmann JS, Bushby K: A gene related to Caenorhabditis elegans spermatogenesis factor fer-1 is mutated in limb-girdle muscular dystrophy type 2B. Nat Genet 1998, 20:37–42
6. Chapman ER, An S, Edwardson JM, Jahn R: A novel function for the second C2 domain of synaptotagmin, Ca2+-triggered dimerization. J Biol Chem 1996, 271:5844–5849
7. Nagaraju K, Rawat R, Veszelovszky E, Thapliyal R, Kesari A, Sparks S, Raben N, Plotz P, Hoffman EP: Dysferlin deficiency enhances monocyte phagocytosis: a model for the inflammatory onset of limb-girdle muscular dystrophy 2B. Am J Pathol 2008, 172:774–785
8. Vandré DD, Ackerman WE 4th, Kniss DA, Tewari AK, Mori M, Takizawa T, Robinson JM: Dysferlin is expressed in human placenta but does not associate with caveolin. Biol Reprod 2007, 77:533–542
9. Gayathri N, Alefia R, Nalini A, Yasha TC, Anita M, Santosh V, Shankar SK: Dysferlinopathy: spectrum of pathological changes in skeletal muscle tissue. Indian J Pathol Microbiol 2011, 54: 350–354
10. Lennon NJ, Kho A, Bacskai BJ, Perlmutter SL, Hyman BT, Brown RH Jr.: Dysferlin interacts with annexins A1 and A2 and mediates sarcolemmal wound-healing. J Biol Chem 2003, 278: 50466–50473
11. Huang Y, Laval SH, van Remoortere A, Baudier J, Benaud C, Anderson LV, Straub V, Deelder A, Frants RR, den Dunnen JT, Bushby K, van der Maarel SM: AHNAK, a novel component of the dysferlin protein complex, redistributes to the cytoplasm with dysferlin during skeletal muscle regeneration. FASEB J 2007, 21: 732–742
12. Matsuda C, Hayashi YK, Ogawa M, Aoki M, Murayama K, Nishino I, Nonaka I, Arahata K, Brown RH Jr.: The sarcolemmal proteins dysferlin and caveolin-3 interact in skeletal muscle. Hum Mol Genet 2001, 10:1761–1766
13. Cai C, Weisleder N, Ko JK, Komazaki S, Sunada Y, Nishi M, Takeshima H, Ma J: Membrane repair defects in muscular dystrophy

are linked to altered interaction between MG53, caveolin-3, and dysferlin. J Biol Chem 2009, 284:15894–15902
14. Jaiswal JK, Marlow G, Summerill G, Mahjneh I, Mueller S, Hill M, Miyake K, Haase H, Anderson LV, Richard I, Kiuru-Enari S, McNeil PL, Simon SM, Bashir R: Patients with a non-dysferlin Miyoshi myopathy have a novel membrane repair defect. Traffic 2007, 8:77–88
15. Klinge L, Laval S, Keers S, Haldane F, Straub V, Barresi R, Bushby K: From T-tubule to sarcolemma: damage-induced dysferlin translocation in early myogenesis. FASEB J 2007, 21:1768–1776
16. Klinge L, Harris J, Sewry C, Charlton R, Anderson L, Laval S, Chiu YH, Hornsey M, Straub V, Barresi R, Lochmuller H, Bushby K: Dysferlin associates with the developing T-tubule system in rodent and human skeletal muscle. Muscle Nerve 2010, 41:166–173
17. Waddell LB, Lemckert FA, Zheng XF, Tran J, Evesson FJ, Hawkes JM, Lek A, Street NE, Lin P, Clarke NF, Landstrom AP, Ackerman MJ, Weisleder N, Ma J, North KN, Cooper ST: Dysferlin, annexin A1, and mitsugumin 53 are upregulated in muscular dystrophy and localize to longitudinal tubules of the T-system with stretch. J Neuropathol Exp Neurol 2011, 70:302–313
18. Davis DB, Delmonte AJ, Ly CT, McNally EM: Myoferlin, a candidate gene and potential modifier of muscular dystrophy. Hum Mol Genet 2000, 9:217–226
19. Davis DB, Doherty KR, Delmonte AJ, McNally EM: Calcium-sensitive phospholipid binding properties of normal and mutant ferlin C2 domains. J Biol Chem 2002, 277:22883–22888
20. Doherty KR, Cave A, Davis DB, Delmonte AJ, Posey A, Earley JU, Hadhazy M, McNally EM: Normal myoblast fusion requires myoferlin. Development 2005, 132:5565–5575
21. Doherty KR, Demonbreun AR, Wallace GQ, Cave A, Posey AD, Heretis K, Pytel P, McNally EM: The endocytic recycling protein EHD2 interacts with myoferlin to regulate myoblast fusion. J Biol Chem 2008, 283:20252–20260
22. Demonbreun AR, Posey AD, Heretis K, Swaggart KA, Earley JU, Pytel P, McNally EM: Myoferlin is required for insulin-like growth factor response and muscle growth. FASEB J 2010, 24:1284–1295
23. Posey AD Jr., Pytel P, Gardikiotes K, Demonbreun AR, Rainey M, George M, Band H, McNally EM: Endocytic recycling proteins EHD1 and EHD2 interact with fer-1-like-5 (Fer1L5) and mediate myoblast fusion. J Biol Chem 2011, 286:7379–7388
24. Benaud C, Gentil BJ, Assard N, Court M, Garin J, Delphin C, Baudier J: AHNAK interaction with the annexin 2/S100A10 complex regulates cell membrane cytoarchitecture. J Cell Biol 2004, 164:133–144
25. Ho M, Post CM, Donahue LR, Lidov HG, Bronson RT, Goolsby H, Watkins SC, Cox GA, Brown RH Jr.: Disruption of muscle membrane and phenotype divergence in two novel mouse models of dysferlin deficiency. Hum Mol Genet 2004, 13:1999–2010
26. Pisani DF, Bottema CD, Butori C, Dani C, Dechesne CA: Mouse model of skeletal muscle adiposity: a glycerol treatment approach. Biochem Biophys Res Commun 2010, 396:767–773
27. Krolenko SA, Amos WB, Brown SC, Tarunina MV, Lucy JA: Accessibility of T-tubule vacuoles to extracellular dextran and DNA: mechanism and potential application of vacuolation. J Muscle Res Cell Motil 1998, 19:603–611
28. Engel WK, Bishop DW, Cunningham GG: Tubular aggregates in type II muscle fibers: ultrastructural and histochemical correlation. J Ultrastruct Res 1970, 31:507–525
29. Chevessier F, Bauche-Godard S, Leroy JP, Koenig J, Paturneau-Jouas M, Eymard B, Hantai D, Verdiere-Sahuque M: The origin of tubular aggregates in human myopathies. J Pathol 2005, 207:313–323
30. Niakan E, Harati Y, Danon MJ: Tubular aggregates: their association with myalgia. J Neurol Neurosurg Psychiatry 1985, 48:882–886
31. Boncompagni S, Protasi F, Franzini-Armstrong C: Sequential stages in the age-dependent gradual formation and accumulation of tubular aggregates in fast twitch muscle fibers: SERCA and calsequestrin involvement. Age (Dordr) 2012, 34:27–41
32. Krolenko SA, Adamian S: [Stereologic analysis of vacuolization of the T-system of frog muscle fibers, detected using confocal fluorescence microscopy] Russian. Tsitologiia 2000, 42:1125–1133
33. Esenberg B, Eisenberg RS: Selective disruption of the sarcotubular system in frog sartorius muscle: a quantitative study with exogenous peroxidase as a marker. J Cell Biol 1968, 39:451–467
34. Sheikh SM, Skepper JN, Chawla S, Vandenberg JI, Elneil S, Huang CL: Normal conduction of surface action potentials in detubulated amphibian skeletal muscle fibres. J Physiol 2001, 535:579–590
35. Schenk D, Barbour R, Dunn W, Gordon G, Grajeda H, Guido T, Hu K, Huang J, Johnson-Wood K, Khan K, Kholodenko D, Lee M, Liao Z, Lieberburg I, Motter R, Mutter L, Soriano F, Shopp G, Vasquez N, Vandevert C, Walker S, Wogulis M, Yednock T, Games D, Seubert P: Immunization with amyloid-beta attenuates Alzheimer-disease-like pathology in the PDAPP mouse. Nature 1999, 400:173–177
36. Davey DF, Dulhunty AF, Fatkin D: Glycerol treatment in mammalian skeletal muscle. J Membr Biol 1980, 53:223–233
37. Zhang H, Wang Y, Li J, Yu J, Pu J, Li L, Zhang S, Peng G, Yang F, Liu P: Proteome of skeletal muscle lipid droplet reveals association with mitochondria and apolipoprotein a-I. J Proteome Res 2011, 10:4757–4768
38. Krolenko SA, Lucy JA: Reversible vacuolation of T-tubules in skeletal muscle: mechanisms and implications for cell biology. Int Rev Cytol 2001, 202:243–298
39. Kerr LM, Sperelakis N: Ca2+-dependent slow action potentials in normal and dystrophic mouse skeletal muscle. Am J Physiol 1983, 245:C415–C422
40. Parton RG, Way M, Zorzi N, Stang E: Caveolin-3 associates with developing T-tubules during muscle differentiation. J Cell Biol 1997, 136:137–154
41. Joe AW, Yi L, Natarajan A, Le Grand F, So L, Wang J, Rudnicki MA, Rossi FM: Muscle injury activates resident fibro/adipogenic progenitors that facilitate myogenesis. Nat Cell Biol 2010, 12:153–163
42. Zechner R, Zimmermann R, Eichmann TO, Kohlwein SD, Haemmerle G, Lass A, Madeo F: FAT SIGNALS–lipases and lipolysis in lipid metabolism and signaling. Cell Metab 2012, 15:279–291
43. Shen X, Franzini-Armstrong C, Lopez JR, Jones LR, Kobayashi YM, Wang Y, Kerrick WG, Caswell AH, Potter JD, Miller T, Allen PD, Perez CF: Triadins modulate intracellular Ca(2+) homeostasis but are not essential for excitation-contraction coupling in skeletal muscle. J Biol Chem 2007, 282:37864–37874
44. Nishi M, Komazaki S, Kurebayashi N, Ogawa Y, Noda T, Iino M, Takeshima H: Abnormal features in skeletal muscle from mice lacking mitsugumin29. J Cell Biol 1999, 147:1473–1480
45. Ito K, Komazaki S, Sasamoto K, Yoshida M, Nishi M, Kitamura K, Takeshima H: Deficiency of triad junction and contraction in mutant skeletal muscle lacking junctophilin type 1. J Cell Biol 2001, 154:1059–1067
46. Lostal W, Bartoli M, Roudaut C, Bourg N, Krahn M, Pryadkina M, Borel P, Suel L, Roche JA, Stockholm D, Bloch RJ, Levy N, Bashir R, Richard I: Lack of correlation between outcomes of membrane repair assay and correction of dystrophic changes in experimental therapeutic strategy in dysferlinopathy. PLoS One 2012, 7:e38036